An integrated hot-rolling and microstructure model for dual-phase steels

D. Bombac[a,*], M. J. Peet[a], S. Zenitani[b], S. Kimura[b], T. Kurimura[b], H. K. D. H. Bhadeshia[a]

[a]*Materials Science and Metallurgy, University of Cambridge, U.K.*
[b]*Hiroshima R&D Center, Mitsubishi Heavy Industries, Ltd., Japan*

Abstract

An integrated tool is presented for the estimation of the microstructure of steels that consist of a mixture of ferrite and martensite following hot deformation processing. The model includes estimation of the effect multi-pass rolling on the austenite size and shape, and its stored energy, information which is then passed on to modules dealing with solid-state phase transformations. Finally, the mechanical properties are estimated using separate modules for strength, toughness and ductility. The integrated model shows good agreement with experimental data.

Keywords: modelling, hot deformation, computational metallurgy, phase structure, overall transformation kinetics

1. Introduction

The mechanical properties of steels are in general sensitive to the processing route so there has been an increasing trend to develop control algorithms for manufacturing equipment such as rolling mills [1–3, for example]. In-

---

*Corresponding author

deed, it places equipment manufacturers at an advantage if they are able to offer algorithms that permit the use to produce specific varieties of steel as a function of equipment settings. The challenge remains to connect existing computerised parameter settings of industrial production equipment to the prediction of properties from metallurgical point of view in all parts of the process [4].

In this paper, a computer aided tool based on mathematical models for prediction of the microstructure and mechanical properties as a function of the hot rolling and cooling conditions is proposed for dual phase steels. An integrated tool proposed for final phase constitution of dual-phase steel has been developed, modelling recrystallization resulting from hot deformation, quantitative microstructure of deformed grains, and structure calculations based on kinetic theory to obtain final microstructure after cooling. At the end, it will be demonstrated that mechanical properties can be predicted with good accuracy from a combination of the measured or calculated structure in combination with a neural network model [5, 6] or other methods that are simpler although linear [7].

2. Integrated tool for prediction of properties

2.1. Hot deformation of austenite

Hot deformation is the standard processing route for steels following casting. For flat products, such as those of interest here, hot rolling is applied while the steel is austenitic. Deformation can be completed at a temperature that leaves the austenite in a plastically deformed condition, because this leads to a refinement of the microstructure that evolves during cooling. The

defects that are introduced into the austenite, during deformation, together with the fact that the austenite surface per unit volume is increased by plastic strain, contribute to the transformation rate for diffusional transformations, and hence enhance both the nucleation and growth rates for ferrite formation. Designating ΔG_S as the stored energy of the austenite, the net driving force becomes:

$$\Delta G \ = \Delta G^{\gamma \to \alpha + \gamma'} + \Delta G_S \qquad \text{diffusional transformation}$$

$$\Delta G \qquad = \Delta G^{\gamma \to \alpha} \qquad \text{displacive transformation}$$

where $\Delta G^{\gamma \to \alpha'}$ and $\Delta G^{\gamma \to \alpha}$ represent the driving forces for the respective reactions. In contrast displacive transformations inherit the defect structure of the parent phase and hence ΔG_S does not contribute to the driving force of transformations.

Plastic deformation leads also to a change in surface energy per unit volume S_V which depends upon the exact nature of the strain, and can be calculated for a variety of deformation methods including rolling, forging and extrusion, using appropriate equivalent strain and quantitative treatment of the topology of deformed grains [8–10].

2.1.1. Static and Metadynamic Recrystallization and Grain Growth

The recrystallization of austenite during hot working has been studied extensively [11–16]. Recovery is the main softening mechanism below a critical strain, and recrystallization occurs only when that strain is exceeded. The critical strain to induce recrystallization depends on initial grain size, strain rate and temperature. For example, when strain rate increases, critical strain for recrystallization also increases. Recrystallization occurs during deforma-

3

tion is called dynamic [17]. Hot strip rolling involves strain rates $> 100\,\mathrm{s}^{-1}$ while interpass times are $< 3\,\mathrm{s}$, which makes dynamic recrystallization unlikely. In multi-pass hot-strip rolling, stored energy due to incomplete softening in preceding passes is accumulated and if this reaches the critical value then recrystallization follows, i.e., metadynamic recrystallization occurs after the final pass or between passes if interpass times are sufficient [18].

Many of the phenomena can be rationalised in terms of a Zener-Holomon parameter [19] that accounts for both temperature and strain rate:

$$Z = \dot{\varepsilon} \exp\left(\frac{Q}{RT}\right) = A \sinh^n\left(\phi\sigma\right) \tag{1}$$

where $\dot{\varepsilon}$ is strain rate, Q is an activation energy for deformation, T is the temperature, A, n, ϕ are material constants and σ is the stress.

An initial model was developed for plate rolling and DRX was neglected due to the relatively small ($\approx 20\%$) reductions of interest in the present work [13]. However, the reductions are greater in strip-rolling passes where DRX needs to be accounted for. Further development included a more detailed interpretation of processes occurring during hot deformation [20]. The critical strain was taken to occur at 0.8 of the strain at peak stress (ε_p) and was described as a function of the initial grain size (d_0 /μm) and Zener-Hollomon parameter (Z /s^{-1}) which describes strain rate and temperature. Peak stress is given as [20]

$$\varepsilon_p = 6.97 \times 10^{-4} d_0^{0.3} Z^{0.17} \tag{2}$$

The kinetics of recrystallization can be reasonably well described by an empirical application of the classical Johnson-Mehl-Avrami-Kolmogorov the-

4

ory [21–23]:

$$X_{\mathrm{RX}} = 1 - \exp\left[-0.693\left(\frac{t}{t_{0.5}}\right)^n\right] \tag{3}$$

where n is material constant and $t_{0.5}$ is the time in seconds for the 50 % recrystallization. For example, time for 50 % recrystallization in C-Mn steels during hot rolling obtained by empirical equations

$$t_{0.5} = 2.5 \times 10^{-19} d_0^2 \varepsilon^{-4} \exp(Q/RT) \qquad \text{for} \qquad \varepsilon \leq 0.8\varepsilon_p \tag{4}$$

$$t_{0.5} = 1.06 Z^{-0.6} \exp(Q/RT) \qquad \text{for} \qquad \varepsilon \geq 0.8\varepsilon_p \tag{5}$$

where d_0 is initial grain size in μm, Q is an activation energy (for C-Mn steels $Q \approx 300$ kJ mol^{-1}) [24], T is absolute temperature in K, Z is Zener-Hollomon parameter in s^{-1}. For typical time intervals of 1 s to 10 s between rolling passes, it can be seen that for C-Mn steel recrystallization typically takes place between each pass for most of the temperature range. At the end of recrystallization, grain size can be for C-Mn steels [20], calculated using

$$d_{\mathrm{rex}} = 0.5 d_0^{0.67} Z^0 \varepsilon^{-1} \qquad \text{for} \qquad \varepsilon \leq \varepsilon^* \tag{6}$$

$$d_{\mathrm{rex}} = 1.8 \times 10^3 Z^{0.15} \qquad \text{for} \qquad \varepsilon \geq \varepsilon^* \tag{7}$$

where d_0 is initial grain size in μm, Z is Zener-Hollomon parameter in s^{-1} and ε^* is

$$\varepsilon^* = 0.57 d_0^{0.17} \varepsilon_p \tag{8}$$

The empirical parameter ε^* is introduced to deal with the fact that the recrystallized grain size d_{rex} is independent of the Zener-Hollomon parameter Z, i.e., it is proportional to $Z^0 = 1$ [25].

Temp / °C	Strain	Strain rate / s^{-1}	Deformation time / s	50% RX time / s
1000	0.53	46	0.011	0.041
985	0.46	112	0.004	0.013
970	0.39	162	0.002	0.028
965	0.39	331	0.0012	0.021

Table 1: Calculations for the rolling schedule reported by Senuma *et al.* [26].

Tables 1–2 compare the time taken for deformation to the calculated time for 50% recrystallization (RX) to occur for Senuma *et al.* [26] and Suehiro *et al.* [27] rolling schedules found in literature.

After recrystallization is complete, normal grain growth processes take place [28]. The fine grain sizes are unstable and rapid grain growth occurs particularly at high temperatures [24, 29]:

$$d^{10} = d_{\mathrm{RX}}^{10} + A_{\mathrm{gg}}t \exp\left(-Q_{\mathrm{gg}}/RT\right). \tag{9}$$

where A_{gg} is material constant and Q_{gg} is activation energy for grain growth (for C-Mn steels $A = 3.87^{32}$ μm^{10}s^{-1} and $Q_{\mathrm{gg}} \approx 400$ kJ mol^{-1}) [24].

During hot rolling, grain size can be calculated from simple geometrical considerations for plane strain deformation [25]. The limit for completely covering prior grain boundaries with new equiaxed grains is given by

$$d_{\mathrm{RX}} = \frac{d_0}{2}\frac{h_t}{h_0} \tag{10}$$

where h_t and h_0 are the final and initial thickness of rolled plate. Using the von Mises' criterion, complete grain boundary nucleation ($X_{\mathrm{gbs}} = 1$) only

Temp / °C	Strain	Strain rate / s^{-1}	Deformation time / s	50% RX time / s
999	0.57	14	0.04	0.09
977	0.20	23	0.009	0.56
964	0.20	39	0.005	0.006
949	0.32	65	0.004	0.085
934	0.27	108	0.0025	0.15
912	0.22	180	0.0012	0.005

Table 2: Calculations for the rolling schedule reported by Suehiro *et al.* [27].

occurs when

$$d_{\mathrm{RX}} \geq \frac{d_0}{2} \exp\left(-\frac{\varepsilon}{2}\sqrt{3}\right) \tag{11}$$

where ε is the equivalent tensile strain.

Utilizing above equations for C-Mn steel with residual strain 0.3, temperature 850 °C and starting grain size 28 μm grain size evolution is shown in figure 1.

The grain size during and after hot rolling can be calculated using this simple model. The grain size calculated for all passes by implementing the above equations is shown in figure 2, for reduction from 250 mm to final thickness of 20 mm with reduction ratio per pass of 0.15. To demonstrate utilisation of model the initial grain size was varied, and the expected convergence can be observed. Residual strain in austenite after rolling and recrystallization results in stored energy (ΔG_S) and influences later decom-
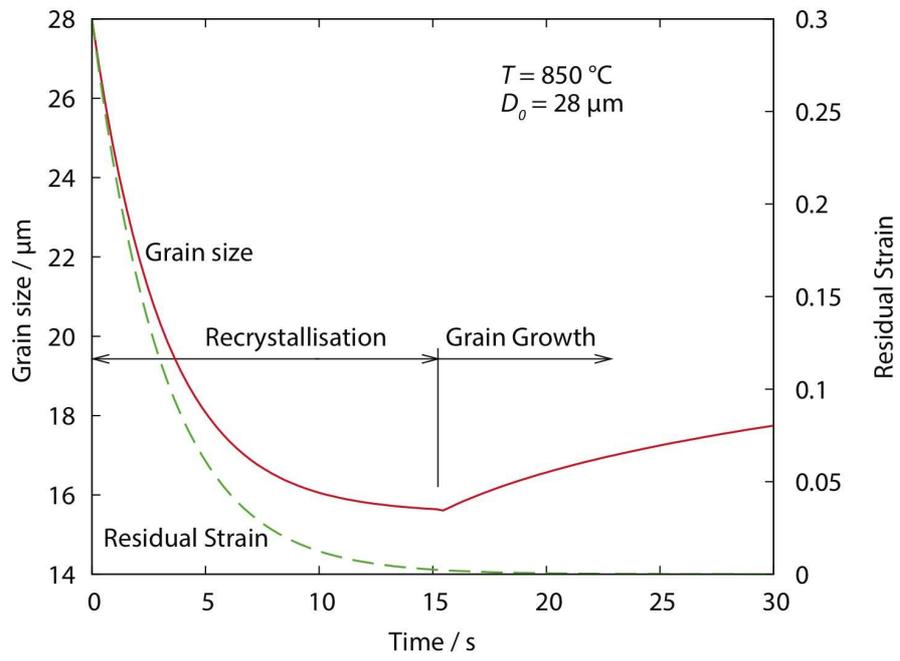
Figure 1: Development of austenite microstructure for C-Mn steel during hot-rolling.
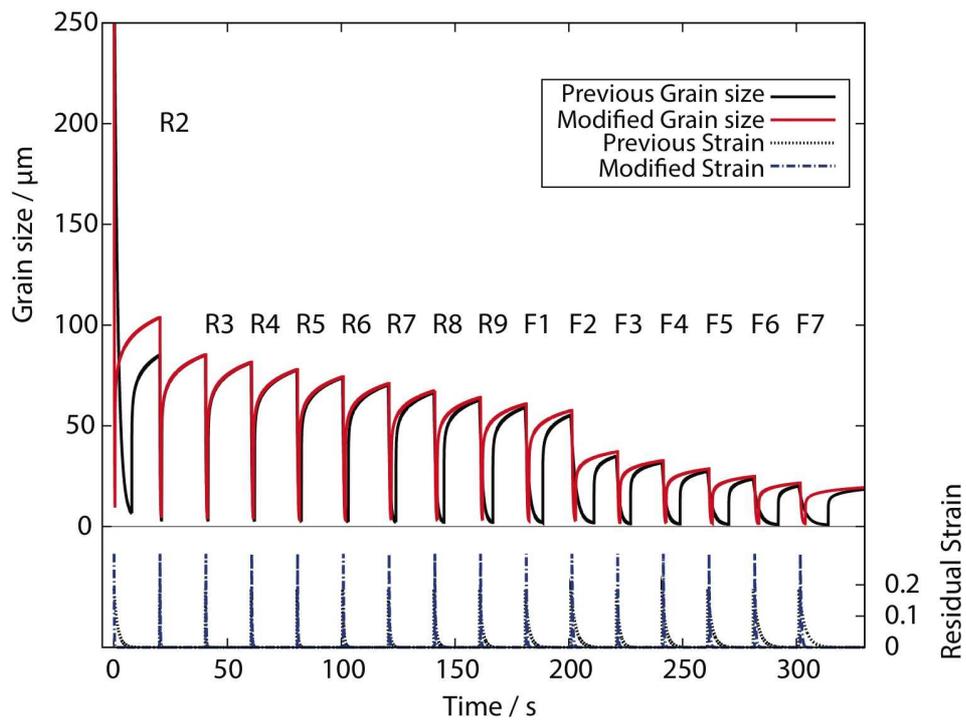
Figure 2: Modification of rolling parameters for first roll pass.

position of austenite into several transformation products. Roughing and finishing passes are marked with R and F, respectively. In connection with data presented in Tables 1–2, the model was also validated for estimation of grain size reported by Senuma *et al.* [26] and Suehiro *et al.* [27] with results graphically presented in figure 3.

2.1.2. Quantitative metallography of deformed grains

During rolling, grains are deformed in the rolling direction more severely than in other directions. This is known as *pancaking*, which increases the amount of boundary per unit volume S_V^{gb}, and therefore the number of nucleation sites for allotriomorphic ferrite. For equiaxed grains, such as fully recrystallised austenite, the surface area per unit volume can be from stereology related to the mean linear intercept grain size, d.

$$S_{V_0} = \frac{2}{d} \tag{12}$$

Implementation of pancaking effect in hot deformation module assumed a tetradecahedron shape, which resembles the true shape of equiaxed grains, and is able to tessellate and fill space in three dimensions [8–10]. The change of surface area per unit volume is for rolling given as [9]

$$\frac{S_V}{S_{V_0}} = \frac{S_{11} + 3\left(S_{11}(1 + 2S_{33}^2)^{1/2} + (S_{11}^2 + 2S_{33}^2)^{1/2}\right) + S_{33}\left(2(1 + S_{11}^2)\right)^{1/2}}{3(2\sqrt{3} + 1)} \tag{13}$$

where S_{11} and S_{33} are principal distortions, i.e. the ratios of the final to initial lengths of unit vectors along the principal axes. Along the principal directions, true strains are given by $\varepsilon_{ii} = \ln(S_{ii})$. It was also shown that application of deformations to the tetradecahedron shape produces essentially

10

(a)

(b)
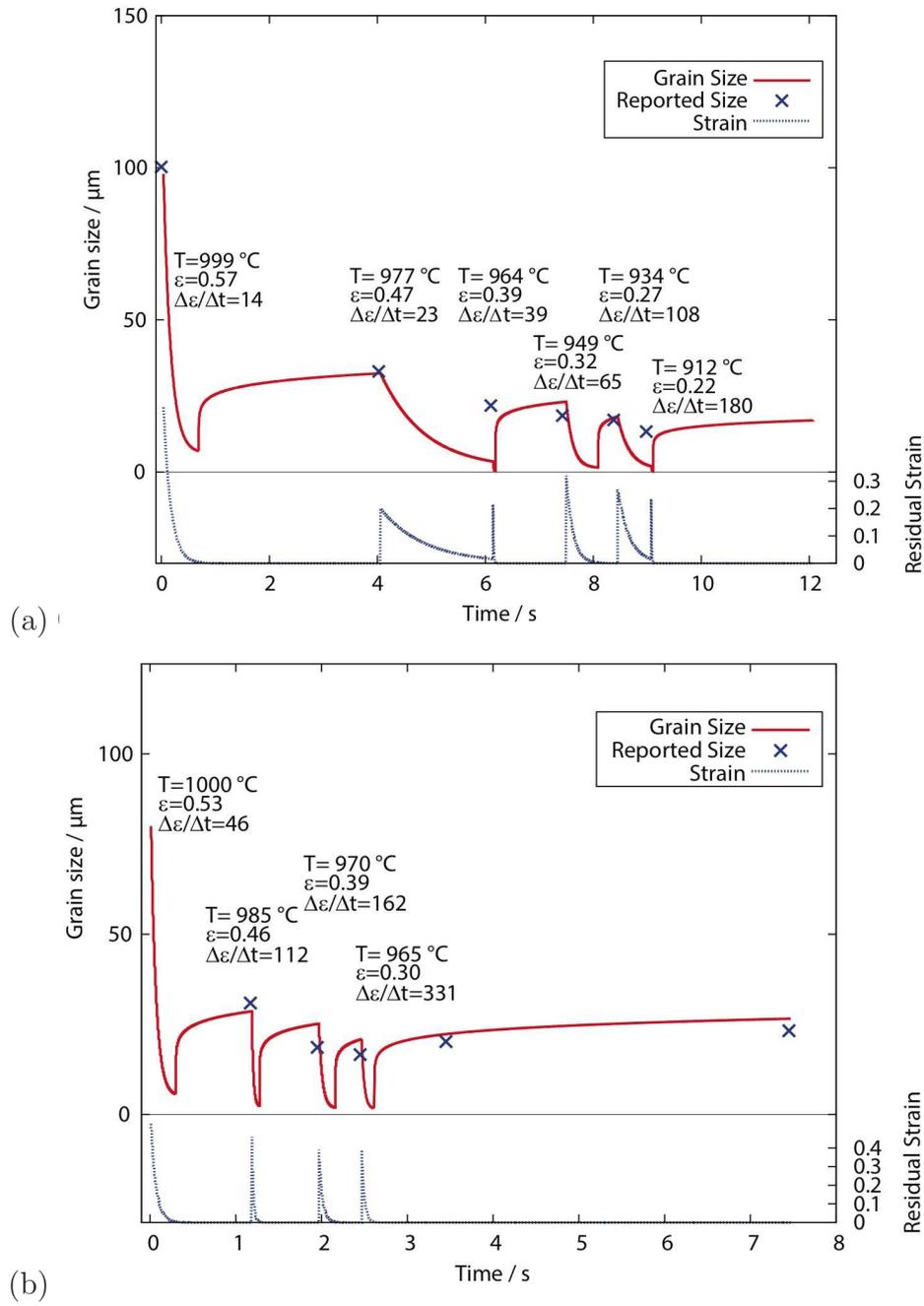
Figure 3: Evolution of grain size during rolling a) rolling schedule after Sneuma *et al.* [26] and b) rolling schedule after Suehiro *et al.* [27].

11

identical results to those produced from stereological measurements [9]. Influence of strain during rolling on the change of surface area per unit volume is depicted in figure 4.
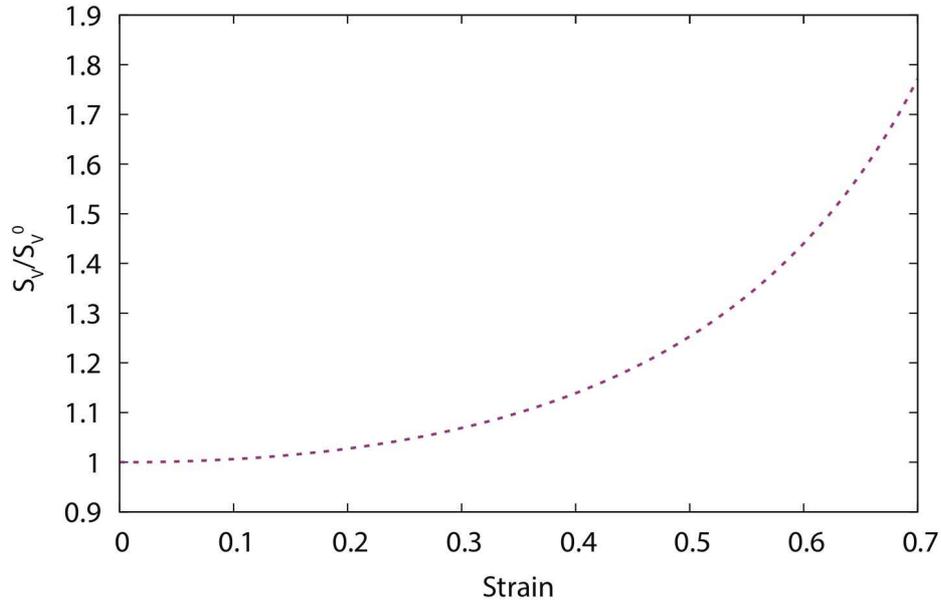
Figure 4: Influence of strain on the change of surface area per unit volume for rolling after equation (13).

2.1.3. Stored energy

Stored energy due to deformation has an influence on the decomposition of austenite during cooling. If the dislocation density is known, energy can be calculated from the length of the dislocation line. It is difficult to measure the dislocation density, therefore a different approach is needed.

The stored energy is calculated as a fraction of the total work done in deformation in the roll passes in which recrystallization did not occur (i.e.,

$n-i$ where n is the number of passes and i the number where recrystallization did occur: $\Delta G_{\text{stored}} = \sum_{n-i}^{n} \alpha_s \overline{\sigma}_i \epsilon_i$, where α_s to be 0.1 [30], so that 10% of the work of deformation is stored. $\overline{\sigma}_i$ and ϵ_i represent the mean stress and strain. This is how the accumulation of strain in the non-recrystallising passes is handled. But the early rolling stages all lead to recrystallization being completed between passes - when recrystallization happens, the stored energy is reset to zero.

As stated above, the stored energy can be estimated by assuming it is 10% of the total work done during deformation [30], which in turn is reduced to the area under the flow stress curve. This can be calculated either empirical or using neural network models. The model was constructed so that in addition to the strain values which can be calculated, the flow stress is estimated as a function of temperature, strain rate, and composition from Zener-Holomon parameter (cf. equation 1). Implementation in the integrated model to calculate flow stress in the austenitic area is based on the inputs from the required deformation schedule.

In the case of simple C-Mn steels, the Swift equation which relates stress and strain, is used with material constants derived by Saito *et al.* [31] to describe the hot deformation of austenite. A neural network model [6] was implemented for other cases, where equations are not available in the literature.

Plastic deformation of austenite leads to an increase in the stored energy. Stored energy has great influence on diffusional transformations due to increase of driving force which is considered in module for calculation of thermodynamics and kinetics of solid-state transformations, presented in

next section. The effect of stored energy on the ferrite grain size is shown in table 3. In the next section it will be demonstrated that increased stored energy (driving force) reduces the ferrite grain size. The more important influence of increasing the stored energy is the greater volume fraction of ferrite transformation. This leads to higher levels of carbon in the austenite and martensite which forms on cooling.

2.2. Phase transformations during cooling

Having defined the state of the austenite, the next stage was to calculate the structure that evolves during cooling. A self contained model where transformations are treated as occurring under paraequilibrium conditions, good approximation for practical circumstances, has been used in the integrated tool to express the decomposition of austenite.

The model considers transformation to allotriomorphic ferrite, pearlite, Widmanstätten ferrite, and martensite. Allotriomorphic ferrite in the model grows under a diffusion-controlled mechanism, and Widmanstätten ferrite is a displacive transformation occurring under paraequilibrium conditions, governed by the diffusion of carbon in the austenite ahead of the plate tip [32, 33]. The calculations include nucleation theory with appropriate considerations made for displacive and diffusional transformations, incorporated into a framework of overall transformation kinetics, taking into account hard impingement between independently nucleated transformation products. The changes in composition of the austenite as transformation evolves are accounted by a mean field. For overall transformation kinetics we use an adaptation of the Johnson-Mehl-Avrami-Kolmogorov theory which accounts for the simultaneous growth of different phases. Alloying elements which are

14

included in the calculations are C, Mn, Si, Ni, Mo, Cr and V, all in solid solution.

2.2.1. Structure calculation

The model for phase transformations uses the extended space method developed originally by Johnson-Mehl-Avrami-Kolmogorov, as adapted later for multiple transformations occurring simultaneously [32, 33]. The implementation requires numerical solution in order, for example, to allow for soft impingement effects and other changing boundary conditions as the austenite decomposes. The equations for nucleation and growth assume there is an unlimited 'extended' volume for transformation, and therefore impingement is accounted for explicitly by further equations. Impingement in real space accounts for the fact that nucleation and growth cannot take place in the regions that have already transformed. To obtain the transformed volume, the extended volume is therefore adjusted according to the untransformed volume fraction.

For transformation from one parent phase into several different daughter phases m, the change in volume of phase j is described by;

$$\mathrm{d}V_j = \left(1 - \frac{\sum_{j=1}^m V_j}{V_{\mathrm{tot}}}\right)\mathrm{d}V_j^e \tag{14}$$

where $\mathrm{d}V$ and $\mathrm{d}V^e$ represent the real and extended changes in volume, and V_{tot} is the total volume of the transforming system. For each phase the nucleation rate I per unit volume, and the growth rate G can be calculated depending on the mechanism For example, when G and I are constant,

$$V_j^e = gV_{\mathrm{tot}} \int_0^t G^3 I(t-\tau)^3 \mathrm{d}\tau \tag{15}$$

15

where τ is an incubation time, and g is a geometric factor, $4/3\pi$ for a spherical particle. The nucleation and growth rates are not of course constant in reality, but the details are described elsewhere [32, 33].

Indeed, the structure calculation model accounts for nucleation at grain boundaries and inclusions, in the former case using the theory developed by [34]. Phases grow on the grain boundary and perpendicularly into the grain. In extended space, the grain boundary can be visualised as a plane, and the grain volume as a series of parallel planes, with distance Δy between each plane. All nucleation takes place on the grain boundary, and impingement must be considered on the grain boundary and in all planes. Considering increase by small finite transformation volume ΔO equation 14 becomes

$$\Delta O_{j,y} = \left(1 - \frac{\sum_{j=1}^{3} O_{j,y}}{O_B} \Delta O_{j,y}^{e} \right) \tag{16}$$

where the subscript y denotes the distance of the plane to the grain boundary, O_B is the total grain boundary area per unit volume, $O_{j,y}$ the transformed area and $\Delta O_{j,y}^{e}$ the extended area of phase j on plane y that is transformed in one time step Δt. If the grain boundary is assumed to be flat then the true volume can be calculated

$$\Delta V_j = \Delta y \sum_{y=0}^{y_{\max}} \Delta O_{j,y} \tag{17}$$

Combining with models for nucleation and growth, then using finite steps, the integral in equation 15 becomes a sum of all n_t time steps so that $t = n_t \Delta t$

$$\Delta O_{j,y}^{e} = O_{\mathrm{B}} \sum_{l=0}^{n_t} A_{j,y,l} \Delta t I_{j,l} \Delta \tau \tag{18}$$

where $A_{j,y,l}$ is the area growth rate for a particle of phase j nucleated at time $\tau = l\Delta\tau$ on plane y and I_j, l the nucleation rate per unit area at this time

16

for phase j. The growth rate of all the particles nucleated between $t = 0$ and time t is calculated by multiplying their number (determined by nucleation rate and nucleation time) with their growth rate at the each plane. Details of the nucleation and growth models for the different phases can be found elsewhere [33].

Chemical segregation causes microstructural banding and needs to be dealt with in structure calculations. In dual-phase steels, Mn fluctuations are known to occur, and are dealt with in our model by assigning different concentration as a function of position [35]. The amplitude of the fluctuation of manganese was set from the average composition and the expected fluctuation. The transformation kinetics are considered at equally spaced positions over one half of the wavelength of the fluctuation. The concentration of the five slices used are calculated using the sinusoidal function.

$$C_{\mathrm{Mn}}(x) = C_0, \mathrm{Mn} - \Delta C_{\mathrm{Mn}} \cos \left(\frac{x-1}{n} \pi \right)$$ (19)

The ferrite grain size d_α is estimated at the end of structure calculation for each slice independently as

$$d_\alpha = \left(\frac{2}{3 N_{v,\alpha}} \right)^{\frac{1}{3}}$$ (20)

where $N_{v,\alpha}$ is total number of allotriomorphic ferrite particles per unit volume [36]. In the program number of ferrite nuclei $N_{v,\alpha}$ is calculated by multiplying the total number of nuclei on one plane with the untransformed area fraction on this plane and summing over all planes

$$N_{v,\alpha} = \sum_k^n N_{v,\alpha,k} \left(1 - \frac{\sum_{j=1}^3 O_{j,k}}{O_B} \right)$$ (21)

17

where $N_{v,\alpha,k}$ is the total number of nuclei on plane k and n is number of all planes [35].

Table 3 shows the effect of stored energy on estimation of ferrite grain size, M_S temperature, volume fraction of ferrite and volume fraction of retained austenite for an alloy Fe-0.1C-0.31Si-1.42Mn wt% with prior austenite grain size 50 μm, cooled at $1\,°\mathrm{C}\,\mathrm{s}^{-1}$.

Table 3: Effect of stored energy for a Fe-0.1C-0.31Si-1.42Mn wt%, austenite grain size 50 μm, cooled at $1\,°\mathrm{C}\,\mathrm{s}^{-1}$, V_α and V_γ are volume fraction of ferrite and retained austenite transformed.

Stored Energy /J mol^{-1}	Ferrite grain size /μm	Carbon in Austenite /wt%	M_S / °C	V_α	V_γ
0	4.85	0.356	343	0.74	0.008
35	4.56	0.409	324	0.78	0.009
70	4.37	0.475	298	0.81	0.01

Figure 5 shows influence of stored energy and austenite grain size on estimation of ferrite grain size for cooling rates $0.1\,°\mathrm{C}\,\mathrm{s}^{-1}$ and $10\,°\mathrm{C}\,\mathrm{s}^{-1}$ for a Fe-0.1C-0.31Si-1.42Mn wt% alloy. Notice the different trends observed for the low and high cooling rates. This is because the model correctly captures the fact that at low cooling rate which is two orders of magnitude smaller than the higher one, the transformation occurs at small undercoolings (high temperatures) so that few nuclei form. These few nuclei can therefore grow rapidly to a size greater than the austenite grain size $\overline{L}_\gamma$, as seen in
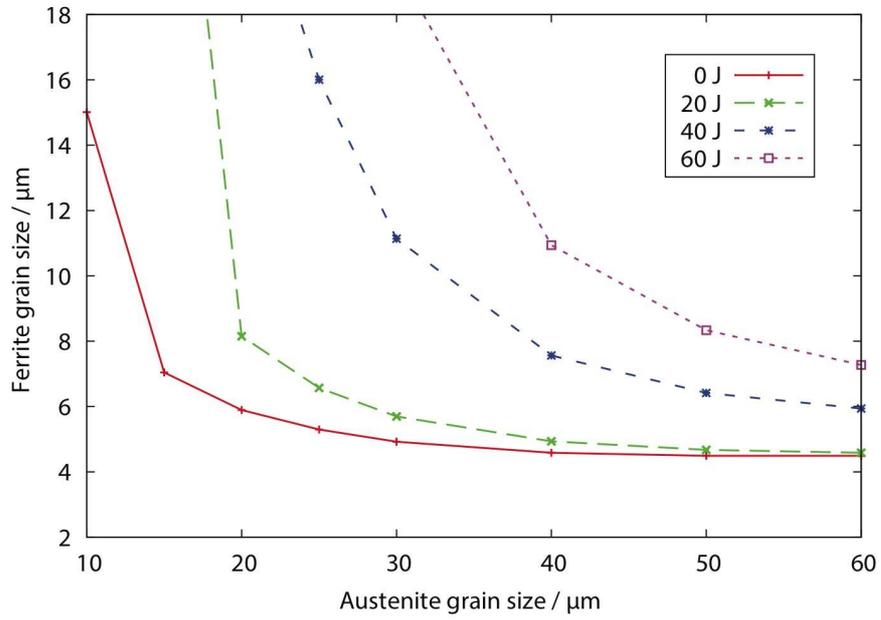
(a)
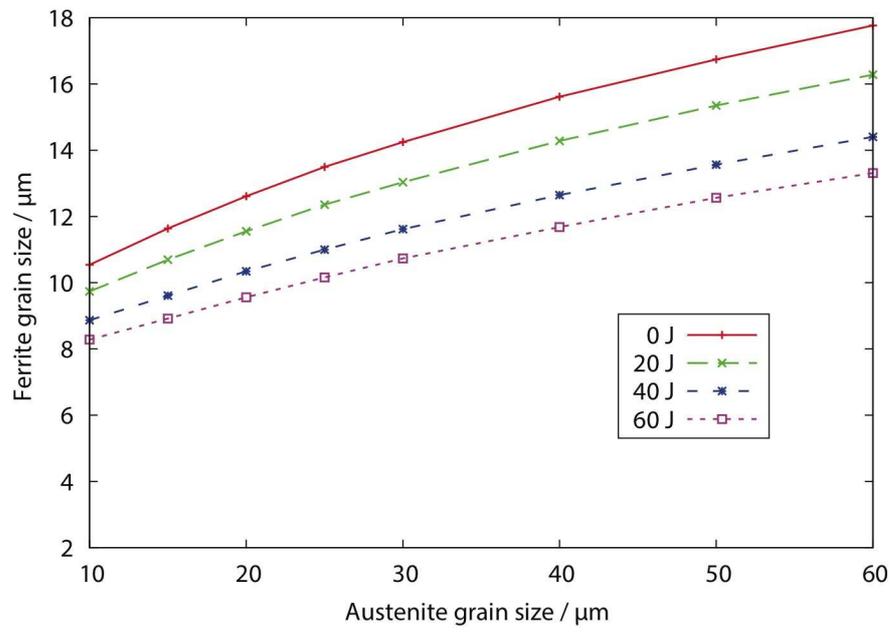
(b)

Figure 5: Estimated ferrite grain size for a Fe-0.1C-0.31Si-1.42Mn wt% alloy as a function of cooling rate, stored energy and prior austenite grain size at cooling rate a) $0.1\,^{\circ}\mathrm{C}\,\mathrm{s}^{-1}$ and b) $10\,^{\circ}\mathrm{C}\,\mathrm{s}^{-1}$.

Fig. 5a. However, as $\overline{L}_\gamma$ increases, the few nuclei simply grow along the austenite boundaries to form layers and then thicken as one-dimensional diffusion-controlled growth, which rapidly slows down with time due to the accumulation of solute ahead of the interface. This means that the grain size then becomes insensitive to $\overline{L}_\gamma$ as seen in Fig. 5a.

At high cooling rates (large undercooling), the nucleation rate is larger, and the greater number density of sites associated with small $\overline{L}_\gamma$ therefore leading to a smaller ferrite grain size, as illustrated in Fig. 5b.

3. Integration of models for prediction of properties

Models presented above treat only separate parts of complex steel processing route. In order to obtain full description at the end of the processing, models were amalgamated as larger modules and integrated in a unified prediction tool. Each component used to build the integrated prediction tool were previously independently verified and validated [8–10, 14–16, 31–33, 35, 37, 38]. In figure 6 the structure of the integrated tool with components of each module (cf. table 4) is shown as a flow chart. The calculation starts with module for hot deformation where input parameters are austenite grain size and rolling schedule (strain, strain rate, interpass times, number of passes) used to estimate grain size after hot deformation. Outputs are used for topology of deformed grain, and determination of stored energy. The structural description of the austenite is passed to the next step, to the structure calculation module where based on the cooling conditions final microstructure and ferrite grain size are calculated.
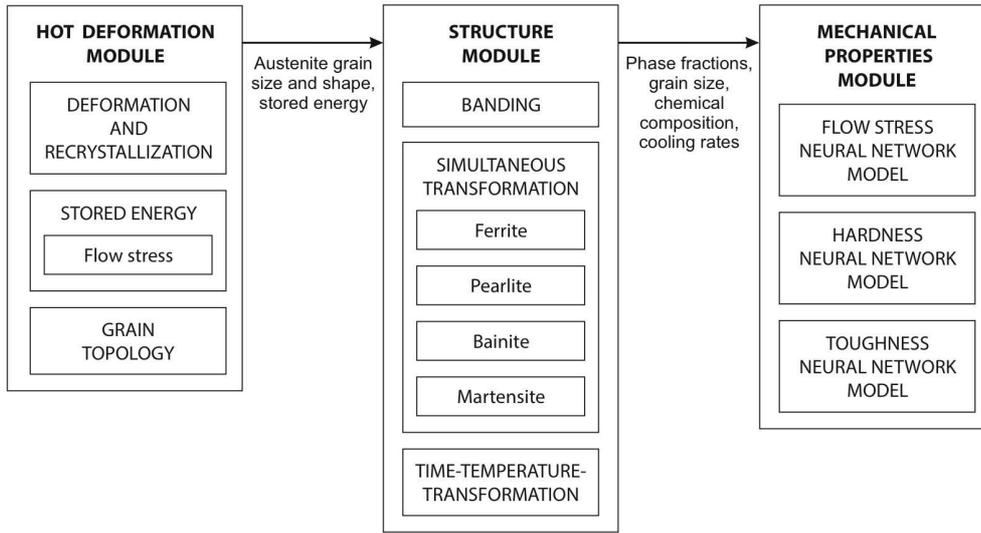
Figure 6: Flow chart of the integrated tool.

Table 4: List of models used in integrated tool.

Hot deformation	Structure calculation	Mechanical properties
Deformation and recrystallization [16, 20, 24]	Banding [35]	Flow stress
Stored energy [6, 31]	Simultaneous transformations [33]	Hardness
Grain topology [8, 9]	Time-Temperature-Transformation [39]	Toughness

4. Experimental validation

The integrated tool presented here can be used for any low-alloy steel, limited only by the phases available in the model. An attempt was made to validate and grade the performance of the calculations with and without deformation for a dual phase steel DP600. Cylindrical samples were machined from a laboratory melt with composition:

Fe-0.115C-0.292Si-1.8Mn-0.513Cr-0.041Al-0.024P-0.007S wt%.

Samples were austenitized at 1173 K for 14 min and cooled with $1\,\mathrm{K\,s^{-1}}$ to 1123 K for 1 min before being cooled to room temperature with three different cooling rates to room temperature. Cooling rates used were $2\,\mathrm{K\,s^{-1}}$, $5\,\mathrm{K\,s^{-1}}$ and $10\,\mathrm{K\,s^{-1}}$. A second set of experiments was conducted with similar temperature programs, however samples were deformed up to strain 0.15 with strain rate $0.1\,\mathrm{s^{-1}}$ at $1123\,\mathrm{K}$, before being cooled. Mica was used to reduce friction between the sample and anvil. As shown in previous work [40] the maximum difference in sample diameter at the anvil and centre is 0.94, and finite element modelling indicated an essentially uniform strain along the centre of specimen, where transformations are measured. Samples were then cut and prepared with standard metallography procedure and etched with 2 % Nital solution for examination with light optical microscope and hardness measurements. Microstructures were quantitatively analysed using the point counting method, table 5 shows the results.

The microstructures are for cooling rates $2\,\mathrm{K\,s^{-1}}$, $5\,\mathrm{K\,s^{-1}}$ and $10\,\mathrm{K\,s^{-1}}$ and no prior deformation shown in figures 7 (a,b,c).

The microstructures of samples where the austenite had been deformed

22
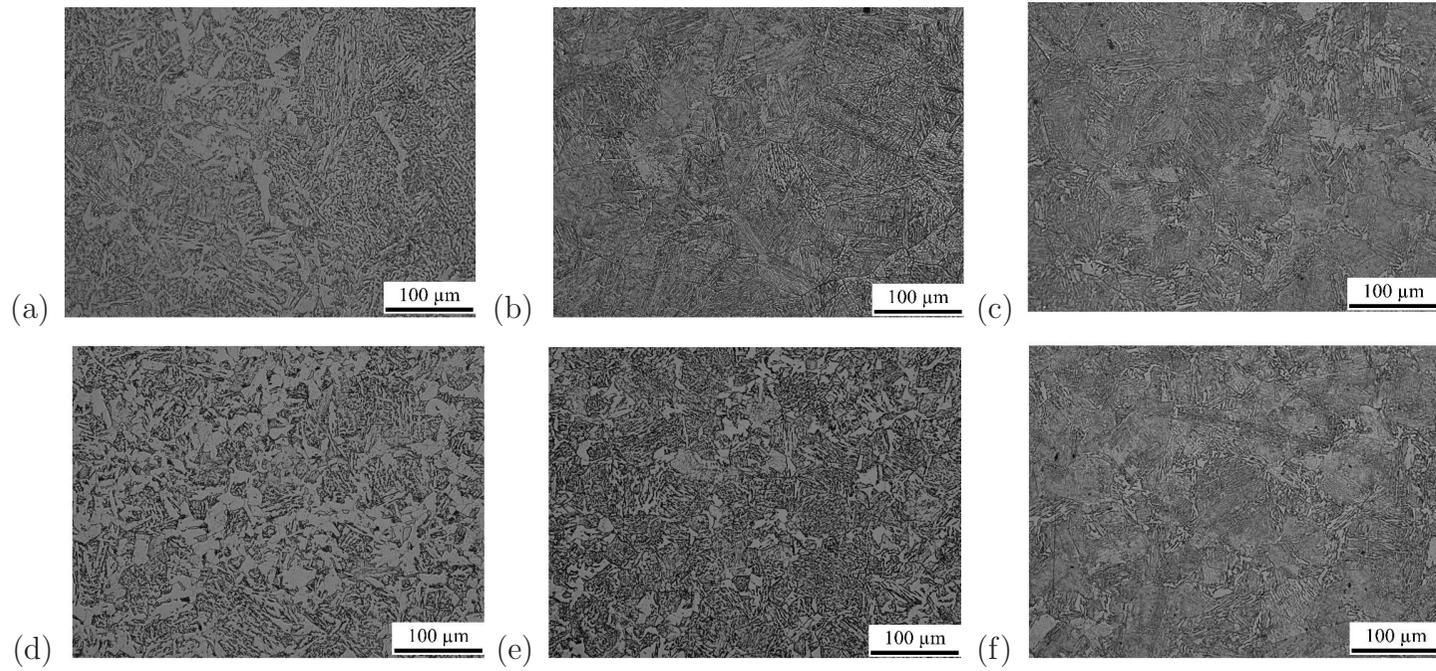
Figure 7: Microstructures obtained at a variety of cooling rates. Samples (a,b,c) are from undeformed austenite and the rest from austenite deformed to a strain of 0.15. a) 2 $\mathrm{K\,s^{-1}}$ $\varepsilon = 0$; b) 5 $\mathrm{K\,s^{-1}}$ $\varepsilon = 0$; c) 10 $\mathrm{K\,s^{-1}}$ $\varepsilon = 0$; d) 2 $\mathrm{K\,s^{-1}}$ $\varepsilon = 0.15$; e) 5 $\mathrm{K\,s^{-1}}$ $\varepsilon = 0.15$; f) 10 $\mathrm{K\,s^{-1}}$ $\varepsilon = 0.15$.

Table 5: Comparison of predicted and calculated amount of ferrite without prior deformation.

Cooling rate /$C\,s^{-1}$	Volume percent ferrite	
	Calculation	Experiment
2	29	33.4 ± 0.2
5	15	10.9 ± 0.2
10	7	10.2 ± 0.2

to a strain of 0.15 are shown in figures 7 (e,f,g) for a variety of cooling rates, and comparisons with calculation are given in table 6.

Table 6: Comparison of predicted and calculated amount of ferrite with deformation up to strain 0.15.

Cooling rate /$C\,s^{-1}$	Volume percent ferrite	
	Calculation	Experiment
2	47	38.3 ± 0.2
5	29	23.7 ± 0.2
10	16	11.6 ± 0.2

The amount of ferrite naturally increases in samples where the transformation occurred from deformed austenite due to the smaller prior austenite grain size and increased stored energy. Comparison between phase calculation for dual phase steel and experimental validation shows that results are in agreement. The model developed here is able to account for all phenomena occurring during hot deformation and predicting phase structure comparable

to experimental results.

5. Summary and conclusions

The integrated model has been developed for the quantitative estimation of steel properties from hot deformation to final microstructure at room temperature. The steel processing route is compartmentalised and models were developed for each step with previous mathematical models connected to the overall scheme to complete the calculations (cf. figure 6). The calculation starts with hot deformation, where important features such as grain size after deformation and recrystallization, amount of boundary per unit volume, stored energy and others are passed on to the structure calculation module where final microstructure and ferrite grain size are calculated. The following conclusions can be reached from the present work:

- The model allows the calculation of austenite during hot deformation and recrystallization. To obtain amount of boundary per unit volume, quantitative metallography of deformed grains is employed.

- Stored energy due to deformation is calculated and considered during transformations during cooling.

- For experimentally evaluated dual phases steel, structure calculation gives results in agreement to experiments.

- The obtained description of microstructure can be easily used for prediction of final mechanical properties with mathematical models or neural network models for specific types of steels.

References

1. D. Sbarbaro-Hofer, D. Neumerkel, and K. Hunt: 'Neural control of a steel rolling mill', *Control Systems, IEEE*, 1993, **13**, 69–75.

2. L. Tang, J. Liu, A. Rong, and Z. Yang: 'A review of planning and scheduling systems and methods for integrated steel production', *European Journal of Operational Research*, 2001, **133**, 1 – 20.

3. D. Bombac, M. Fazarinc, G. Kugler, and R. Turk: 'Tool for programmed open-die forging – case study', *RMZ – Materials and Geoenvironment*, 2008, **55**, 19 – 29.

4. G. J. Schmitz, and U. Prahl: 'Toward a virtual platform for materials processing', *Journal of Metals*, 2009, **61**, 19–23.

5. H. K. D. H. Bhadeshia: 'Neural networks in materials science', *ISIJ International*, 1999, **39**, 966–979.

6. M. Peet: 'Transformation and tempering of low–temperature bainite': Ph.D. thesis, University of Cambridge, Cambridge, U. K., 2010.

7. J. Majta, R. Kuziak, M. Pietrzyk, and H. Krzton: 'Use of the computer simulation to predict mechanical properties of c-mn steel, after thermomechanical processing', *Journal of Materials Processing Technology*, 1996, **60**, 581 – 588.

8. S. B. Singh, and H. K. D. H. Bhadeshia: 'Topology of grain deformation', *Materials Science and Technology*, 1998, **15**, 832–834.

9. Q. Zhu, C. M. Sellars, and H. K. D. H. Bhadeshia: 'Quantitative metallography of deformed grains', *Materials Science and Technology*, 2007, **23**, 757–766.

10. J. Y. Chae, R. S. Qin, and H. K. D. H. Bhadeshia: 'Topology of the deformation of a non–uniform grain structure', *ISIJ International*, 2009, **49**, 115–118.

11. R. A. P. Djaic, and J. J. Jonas: 'Static recrystallization of austenite between intervals of hot working', *Journal of Iron Steel Institute*, 1972, **210**, 256–261.

12. R. A. P. Djaic, and J. J. Jonas: 'Recrystallization of high carbon steel between intervals of high temperature deformation', *Metallurgical Transactions*, 1973, **4**, 621–624.

13. C. M. Sellars, and J. A. Whiteman: 'Recrystallization and grain growth in hot rolling', *Metal Science*, 1979, **13**, 187–194.

14. T. Senuma, H. Yada, Y. Matsumura, and T. Futamura: 'Structure of austenite of carbon steels in high speed hot working processes', *Tetsu–to–Hagane*, 1984, **70**, 2112–2119.

15. H. J. McQueen, and J. J. Jonas: 'Recent advances in hot working: Fundamental dynamic softening mechanisms', *Journal of Applied Metal Working*, 1984, **3**, 233–241.

16. C. M. Sellars: 'Basics of modelling for control of microstructure in thermomechanical control processing', *Ironmaking and Steelmaking*, 1995, **22**, 459–464.

17. G. Kugler, and R. Turk: 'Modeling the dynamic recrystallization under multi-stage hot deformation', *Acta Materialia*, 2004, **52**, 4659 – 4668.

18. R. A. Petkovic, R. A. Luton, and J. J. Jonas: 'Recovery and recrystallization of carbon steel between intervals of hot working', *Canadian Metallurgical Quarterly*, 1975, **14**, 137–145.

19. C. Zener, and J. H. Hollomon: 'Effect of strain rate upon plastic flow of steel', *Journal of Applied Physics*, 1944, **15**, 22–32.

20. C. M. Sellars: 'Modelling microstructural development during hot–rolling', *Materials Science and Technology*, 1990, **6**, 1072–1081.

21. W. A. Johnson, and R. F. Mehl: 'Reaction kinetics in processes of nucleation and growth', *TMS–AIMME*, 1939, **135**, 416–458.

22. M. Avrami: 'Kinetics of phase change 1', *Journal of Chemical Physics*, 1939, **7**, 1103–1112.

23. A. N. Kolmogorov: 'On statistical theory of metal crystallisation', *Izvestiya Akad. Nauk SSSR (Izvestia Academy of Science, USSR)*, 1937, **Ser. Math. 3**, 335–360.

24. C. M. Sellars: 'The physical metallurgy of hot working', In: C. M. Sellars, and G. J. Davies, eds. *Hot Working and Forming Processes*. London, U.K.: Metals Society, 1980: 3.

25. C. M. Sellars: 'The kinetics of softening processes during hot working of austenite', *Czechoslovak Journal of Physics B*, 1985, **35**, 239–248.

26. T. Senuma, M. Suehiro, and H. Yada: 'Mathematical models for predicting microstructural evolution and mechanical properties of hot strips', *ISIJ International*, 1992, **32**, 423–432.

27. M. Suehiro, K. Sato, Y. Tsukano, H. Yada, T. Senuma, and Y. Matsumura: 'Computer modelling of microstructural change and strength of low carbon steel in hot strip rolling', *Trans. ISIJ*, 1987, **27**, 439–445.

28. C. M. Sellars, and J. A. Whiteman: 'Controlled processing of HSLA steels', In: *Product Technology Conference*. Sheffield, U. K.: British Steel Corporation, 1976:.

29. E. Ruibal, J. J. Urcola, and M. Fuentes: 'Static recrystallization kinetics, recrystallized grain size, and grain growth kinetics after hot deformation of a low-alloy steel', *Zeitschrift für Metallkunde*, 1985, **76**, 568–576.

30. X. D. Liu, and P. Karjalainen: 'Effect of processing parameters on the stored energy during multi-pass deformation of a Nb-bearing steel', In: *Proceedings of Conference on Mechanical Working and Steel Processing*, vol. 33. Materials Park, Ohio, USA: AIME, 1996:769–774.

31. Y. Saito, T. Enami, and T. Tanaka: 'The mathematical model of hot deformation resistance with reference to microstructural changes during rolling in plate mill', *Transactions of the Iron and Steel Institute of Japan*, 1985, **25**, 1146–1155.

32. J. D. Robson, and H. K. D. H. Bhadeshia: 'Modelling precipitation

sequences in power plant steels: Part I, kinetic theory', *Materials Science and Technology*, 1997, **13**, 631–639.

33. S. Jones, and H. K. D. H. Bhadeshia: 'Competitive formation of inter- and intragranularly nucleated ferrite', *Metallurgical & Materials Transactions A*, 1997, **28A**, 2005–2103.

34. J. W. Cahn: 'The kinetics of grain boundary nucleated reactions', *Acta Metallurgica*, 1956, **4**, 449–459.

35. E. A. Jägle: 'Modelling of microstructural banding during transformations in steel': Master's thesis, University of Cambridge, Cambridge, U. K., 2007.

36. S. V. Parker: 'Modelling of phase transformations in hot–rolled steels': Ph.D. thesis, University of Cambridge, 1997.

37. F. üthe. Siciliano, and J. Jonas: 'Mathematical modeling of the hot strip rolling of microalloyed Nb, multiply-alloyed Cr-Mo, and plain C-Mn steels', *Metallurgical & Materials Transactions A*, 2000, **31**, 511–530.

38. N. Cabanas, J. Penning, N. Akdut, and B. Cooman: 'High-temperature deformation properties of austenitic Fe-Mn alloys', *Metallurgical & Materials Transactions A*, 2006, **37**, 3305–3315.

39. J. L. Lee, and H. K. D. H. Bhadeshia: 'A methodology for the prediction of time-temperature-transformation diagrams', *Materials Science and Engineering A*, 1993, **A171**, 223–230.

40. P. H. Shipway, and H. K. D. H. Bhadeshia: 'Mechanical stabilisation of bainite', *Materials Science and Technology*, 1995, **11**, 1116–1128.